THREE-DIMENSIONAL ACOUSTIC SIMULATION ON ACOUSTIC SCATTERING BY NONLINEAR INTERNAL WAVE IN COASTAL OCEAN

LINUS Y. S. CHIU, CHI-FANG CHEN

Department of Engineering Science and Ocean Engineering, National Taiwan University
E-mail: cys@uwaclab.na.ntu.edu.tw

JAMES F. LYNCH

Woods Hole Oceanography Institute

Nonlinear internal wave (NIW) packets cause ducting and whispering gallery effects in acoustic propagation. The acoustic energy restricted within the internal wave crests (crest-crest) on the shelf is the ducting effect, and the energy confined along the crest when the source is located upslope from the NIW crest is the whispering gallery effect. This paper presents the simulation results concerning the phenomena of whispering gallery by FOR3D wide-angle version. It appears that energy emerges right before and along the wave crest and then vanish right in the back of the wave crest and then converges again, especially with the lower frequency band (150Hz~ 600Hz).

1 Introduction

The influence on the amplitude and phase of an acoustic field propagating through the shallow water waveguides is significant over relatively short ranges while the sound speed fluctuations in the region are typically less than one percent of the mean speed [1-5]. Our interest in this behavior stems from two points related to underwater communication system or the sonar performance. It is that signal detection is a function of the signal-to-noise ratio and is affected by transmission loss (TL) variability caused by sound speed perturbations with internal wave.

Recent papers and experiments address the acoustic field is fluctuated by the nonlinear internal waves (NIW). We have seen the energy distribution has specified modification due to the acoustic mode coupling while the sound propagates across the internal wave. They also cause ducting and whispering gallery effects as the sound propagates along the internal waves. The acoustic energy restricted within the internal wave crests (crest-crest) is the ducting effect [6], and the energy confined along the crest when the source is located at the upslope region relatives to the NIW crest is called the whispering gallery effect.

Computer simulation offers a practical method for systematic assessment of TL and coherence degradation in complex ocean environments. This approach is applied here, where the TL and azimuthal spatial coherence are estimated for frequencies band of 50-800 Hz as a function of range, depth, and azimuth in shallow water, continental shelf environment under summer condition. Sound speed fluctuations considered in this paper are induced by an internal gravity wave field that perturbs the thermocline. Some recent theoretical efforts have considered the effect of internal wave induced phase decorrelation on horizontal arrays in both deep and shallow water environments under a variety of modeling assumptions [6].

Our analysis differs from those of previous studies in that we employ a simplified, data-constrained internal wave model which is observed in the ASIAEX experiment, South China Sea (SCS) component that includes a azimuthal anisotropic component, and

apply 3D acoustic modeling techniques (FOR3D with wide angle version) to estimate TL and azimuthal coherence in this environment.

This paper presents evidence that acoustic field can be significantly affected in an environment supporting oceanographic features that break azimuthal symmetry. Such affection might not be predicted by *N x*2D calculations since they ignore horizontal refraction and may thus produce misleading TL and azimuthal coherence in these environments. This paper also addresses and quantifies the whispering Gallery Effect induced by the internal solitary wave in the typical continental slope region. We have two basic results:

1. Enhanced energy emerges right before and along the wave crest and then vanishes right in the back of the wave crest and then converges again, especially with the lower frequency band (150Hz~ 600Hz).
2. Scattering of sound due to the internal solitary waves brings about much worse azimuthal coherence in the time scale of 25 minutes. The azimuthal coherence is better in lower frequencies and increasing depth.

In Sec. II we briefly review the simulation scenario and analysis approach. In Sec. III, we give the results and implementation of numerical experiments, which estimate energy distribution in the 3D field, the adaptive depth-averaged acoustic energy and azimuthal coherence under several conditions. The summary and conclusions are presented in Sec. IV.

2 Simulation Approach

Three dimensional effects on underwater acoustic propagation have been frequently reported [7-9]. The acoustic propagation model is based on the 3D parabolic approximation to the Helmholtz equation implemented in the computer code FOR3D [9]. This code implements a finite difference solution scheme, using discretized differential operators to represent wide-angle propagation in elevation and narrow-angle azimuthal coupling. The major causes for the 3D effects are variations in azimuth of bottom topography and/or water column properties [10-13]. Experiment site in South China Sea is of a similar nature, in that both bathymetry and horizontally anisotropic water column properties contribute to horizontal refraction of energy.

Details of the simulation scenario and parameters are given in the Fig.1 (a). The acoustic point source which placed in the upper water column is assumed to be a tow acoustic source. The emitted sound propagates in the wedge bathymetry which slope is equal to the 1/20. Superimposed on the sound speed volume is an observed internal wave in South China Sea which causes very large thermocline depressions even to 85 meters from thermo. Internal wave propagated onshore from 2 kilometers far from the source until the 0.5 kilometers. The dynamic elevations of the internal wave due to the onshore-propagating are ignored in this time scale of only 25 minutes. Finally the bottom parameters are constant in range and selected from a somewhat very hard, sandy bottom. And the density is set to be twice that of the water density.

2.1 Transmission loss

Nonlinear internal wave fields introduce significant azimuthal transfer of energy. Acoustic field calculations performed through a set of 2D range/depth planes (a.k.a. *Nx*2D computations) for different azimuthal directions allow for variations in sound speed within range/depth planes but ignore horizontal refraction of energy between adjacent

planes. The 3D calculations presented here include such azimuthal coupling, if present, and can be used to assess the relative importance of horizontal refraction in complex oceanographic environments. A rather simple means of estimating the amount of azimuthal energy transfer is outlined here and used to interpret TL and coherence results. Define a adaptive depth-averaged acoustic energy density (ADAAE) E:

$$E = E(r,\phi) = \frac{\int_0^H |u|^2 / \rho(z)\,dz}{C_0{}^2 H} \tag{1}$$

where H is the total depth(or arbitrary depth) of water column and sediment, and C_0 is a nominal reference sound speed. The depth averaged, or mean TL, TL_z ([1] and [4]), is

$$TL_z = 10 \log_{10} E \tag{2}$$

where E has unit of energy per area.

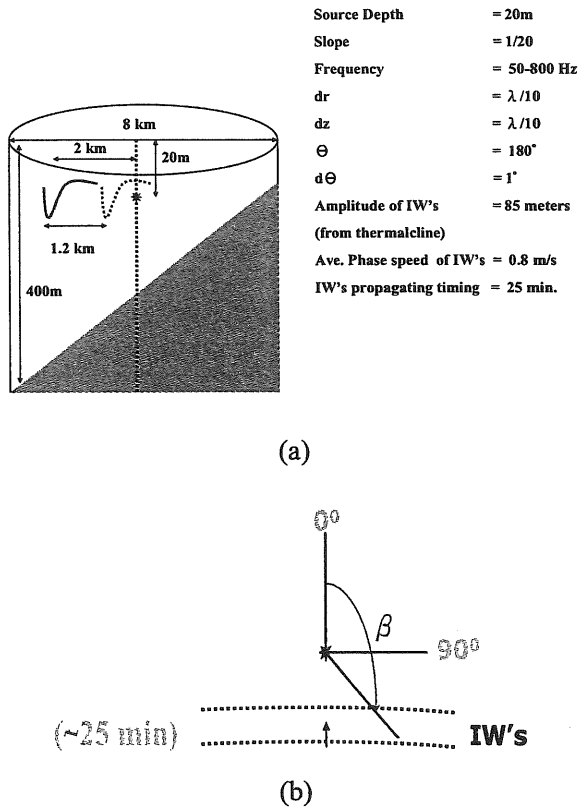

Figure 1. The details of simulation scenario and parameters. Internal wave propagated onshore from 2 kilometers far from the source until the 0.5 kilometers.

2.2 Azimuthal Coherence

Azimuthal coherence is a three-dimensional function which includes the parameters r, z, β (range, depth and azimuth). The complex pressure field $u(r,z,\beta)$ (azimuthally

across the slope) is correlated with its value at $\beta = 0$ (along the slope) and temporally averaged and then normalized as:

$$C_{\vartheta 90^\circ}(r,z,\beta) = \frac{\left|\left\langle u(r,z,90^\circ)u^*(r,z,\beta)\right\rangle\right|}{\sqrt{\left\langle\left|u(r,z,90^\circ)\right|^2\right\rangle\left\langle\left|\ u(r,z,\beta)\ \right|^2\right\rangle}} \tag{3}$$

See also Fig.1 (b). The angle brackets represent the time average over environment snapshot (~25 minutes). This dependence on integration time is due to the non-stationary nature of the sound speed filed induced by the internal waves.

3 Implementation and Results

3.1 Results of Transmission loss

This section presents some results of acoustic calculations for TL, ADAAE, effect of whispering gallery and azimuthal coherence. TL examples presented here are the single environment snapshot while the internal wave is right at 1 km from source and the frequencies are of 50 Hz and 150 Hz. They are shown in Fig.2 (a), (b) as a function of range and azimuth at specified depth. ((a)30 meters, (b)50 meters). The first column in each figure is the case for imposed internal wave; the middle is the case for background sound speed profile (without the internal wave) and the last is the difference between the previous two columns.

In (a) and (b), the middle ones are the typical bench mark of three-dimensional wedge problem. Clear see that energy distribution is no longer circle-like but curved and bend down to the deeper water region. But the internal wave comes in (propagates onshore), they may induce the oceanic waveguide so as to concentrate the energy near or along the boundary, as shown in the left column of Fig. 2. Such concentration of energy near the boundary is completely analogous to the whispering gallery modes. The right column in Fig. 2 shows the enhanced horizontal refraction induced by the internal wave since the phasing and the amplitude of the interference pattern has changed.

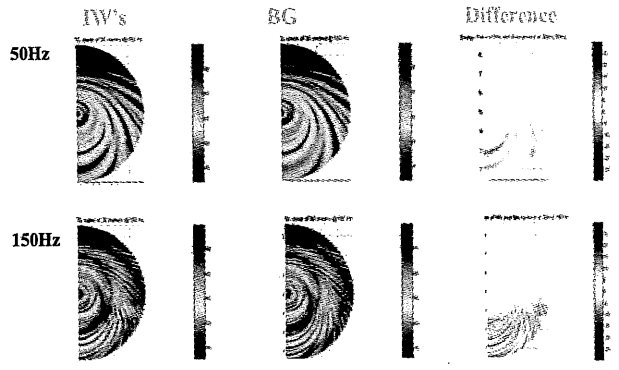

(a)

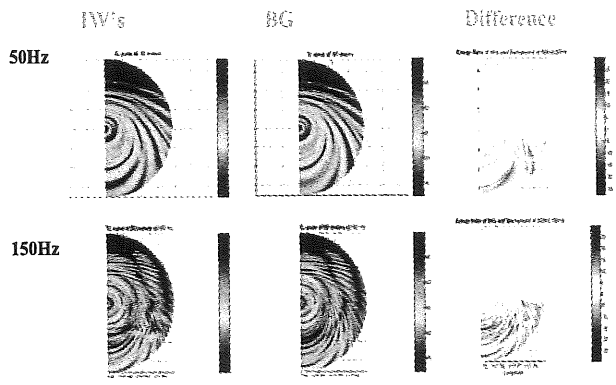

(b)

Figure 2 Transmission losses at specified depths. ((a) 30 meters, (b) 50 meters). The left columns show the case of incoming internal wave; the middle ones are the cases of background sound speed profile and the right ones are the differences.

3.2 Results of ADAAE

In order to clearly see the redistribution of energy caused by the internal wave, the ADAAE is utilized where H = 50 meters and shown in Fig. 3. The averaging depth of 50 meters is chosen to see the acoustic scattering of upper water column induced by the incoming internal wave. Fig. 3(a) and (b) are the cases for increasing frequencies; the cases for the incoming internal wave are shown in the left column and the ones for the background sound speed profile are shown in the right column. Only the results of 150Hz, 200Hz, 700Hz and 800Hz are shown here. Fig.3 illustrates the enhanced energy occurring near and along the boundary which is regarded as the oceanic waveguide induced by the nonlinear internal wave, especially in Fig. 3(a). For lower frequencies (50-600Hz), the modal interference pattern of energy and the scattering effect are clearly seen since the source may excite only lower modes, but the pattern are getting disordered (see Fig.3. (b)) due to the higher modes excited at higher frequencies. The effect of enhanced energy along the boundary of the internal wave has been gradually smeared (not shown here) while the averaging depth is increasing. This tells that the whispering gallery effect mainly occurs in the upper water column so that the effect is smeared with the increasing averaging depth.

3.3 The Effect of Whispering Gallery

The quantity has been defined for describing the effect of whispering gallery since the enhanced energy is horizontally stratified induced by the internal wave. The parameter $WG\ (y_k, w)$ is defined as the function of the distance relative to the source, y_k, and frequencies ϖ, see also Fig. 4.

$$WG(y_k,\varpi) = \frac{\sum_{1}^{N} DAAE_i(y_k,\varpi)}{N},\quad k = 1,2,3,... \tag{4}$$

$$WGL = 10\log_{10}(WG_{IW's}) - 10\log_{10}(WG_{BG}) \tag{5}$$

where the energy distribution of ADAAE is summarized and averaged. Since the $WG\ (y_k, \varpi)$ is to describe the energy horizontally distributed in the computed sound volume while the averaging depth H = 50 meters, the difference between logarithmic scale of $WG\ (y_k, \varpi)$ of the case with imposed internal wave and of the background case can clearly represent the scattering effect induced by the internal wave. Fig.5 clearly displays the effect of whispering gallery along the boundary and the shadow region in the back of wave-crest. Enhanced energy emerges right before and along the wave crest and then vanishes right in the back of the wave crest and then converges again, especially with the lower frequency band (150Hz~ 600Hz).

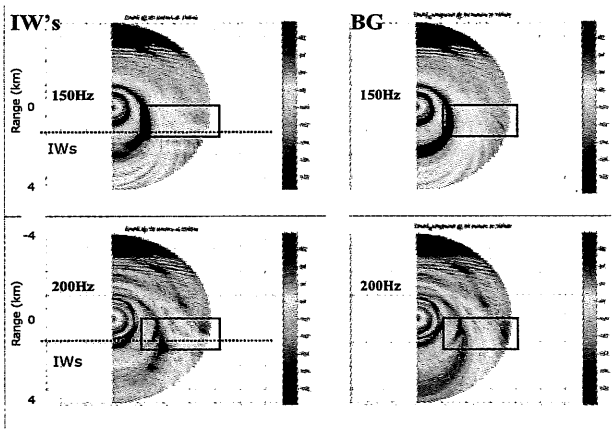

(a)

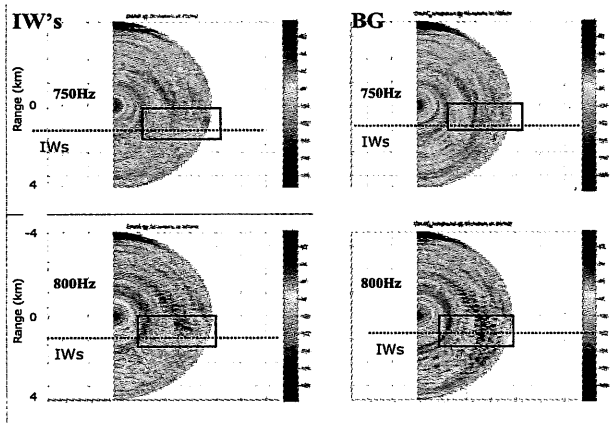

(b)

Figure 3. (a) and (b) are the results of ADAAE for increasing frequencies; the left columns are the results of incoming internal wave and right ones are the results of background sound speed profile. The averaging depths are 50 meters.

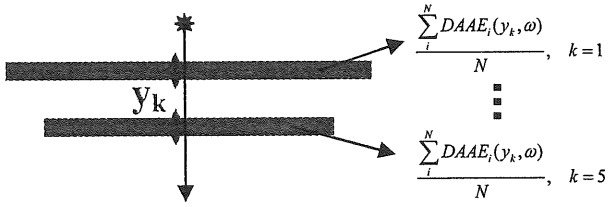

Figure 4. The parameter $WG(y_k, w)$ is defined as the function of the distance relative to the source, y_k, and frequencies ϖ.

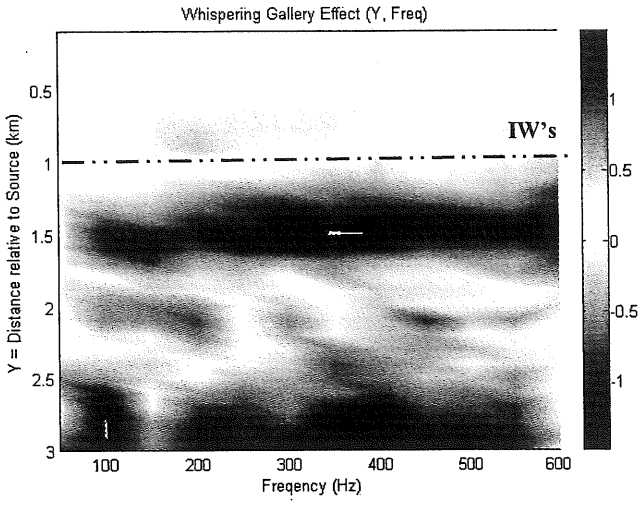

Figure 5. The effect of whispering gallery, a function of y_k and frequencies. Enhanced energy emerges right before and along the wave crest and then vanishes right in the back of the wave crest and then converges again, especially with the lower frequency band (150Hz~ 600Hz).

3.4 Results of Azimuthal Coherence

As shown in Fig.1 (b), the azimuthally coherence is obtained by correlating the complex sound field in each slice of different azimuth with the values of the slice of $u(r, z, 90^\circ)$ and averaged over 25 minutes. The azimuthal coherence is to see the signal coherence between the acoustic channel along the same isobaths of the source and the others which are in the upward (or downward) slope bathymetries. The azimuthally coherence will provide important information for communication or detection about how they treating the targets at different azimuths and evaluating the results, especially in the three-dimensional environment.

Fig. 6(a) and 6(b) show the $C_{\beta 90^\circ}(r,z,\beta)$ results of at $z = 20$ meters and 50 meters with different frequencies. Scattering of sound due to the internal solitary waves brings about the worse azimuthal coherence especially with higher frequencies. Compare the cases between different frequencies in Fig. 6(a) or 6(b), azimuthal coherence is better with lower frequency (even to 0.6 differences at specified range and azimuth) since higher modes excited by high frequencies may cause the disordered interference pattern so that the phasing and the amplitude of the modes would be highly disturbed. This arises the worse azimuthal coherence in higher frequencies. On the other hand, the scattering effect mainly occurs in the upper water column, this may bring about the high coherence in the deeper water (0.6~0.7 difference at deeper water column). Compare Fig. 6(a) with 6(b), the coherence is much better with increasing depth, which is also due to the downward refracting sound speed profiles. This causes that the energy is transferred from high sound speed regions to low sound speed regions so that the deeper water column had higher coherence.

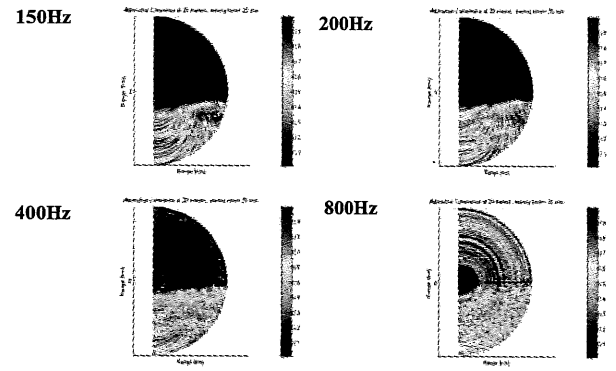

(a)

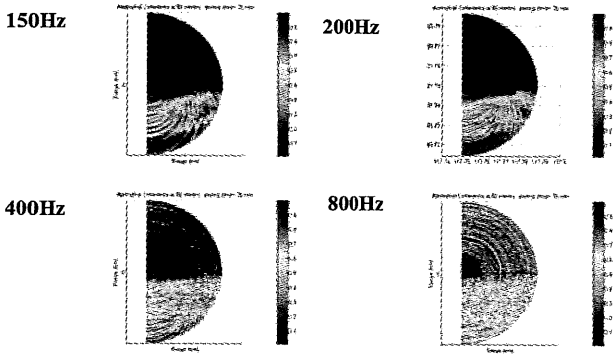

(b)

Figure 6. The results of $C_{\beta 90^\circ}(r,z,\beta)$ at 20 meters (a) and 50 meters (b) with different frequencies. Azimuthal coherence is better with lower frequency and with increasing depth.

4 Summary and Conclusions

This paper describes results of fully 3D numerical experiment involving the acoustic wave fields through a dynamic, 3D oceanographic environment in a typical continental slope region. The environments consists of both dominate summer sound speed profile and the observed internal wave in South China Sea which causes strongly thermocline depressions. A fully 3D parabolic code (FOR3D) with wide angle version is used to compute the transmission loss in the band from 50Hz to 800Hz, the adaptive depth average acoustical energy and the azimuth coherence which is the time-dependent function. The internal wave in the continental slope brings about the enhanced energy emerging along or near the wave since the wave crest induces the oceanic waveguide.

Such concentration of energy near the boundary is completely analogous to the whispering gallery modes. The simulation reveals that the space-time structure of an acoustic field can be significantly altered in this type of oceanographic environment for some propagation conditions. This would not be predicted on the basis of 2D or Nx2D calculations since those calculations ignore the azimuthally coupling.

ADAAE is utilized to clearly see the redistribution of energy caused by the internal wave but not only choose one specified depth. The effect of enhanced energy along the boundary of the internal wave has been gradually smeared (not shown here) while the averaging depth is increasing. This tells that the effect of the whispering gallery or the scattering by the internal wave mainly occurs in the upper water column so that the effect is smeared with increasing the averaging depth. The parameter $WG\ (y_k, w)$ clearly displays the effect of whispering gallery along the boundary and the shadow region in the back of wave-crest. Enhanced energy emerges right before and along the wave crest and then vanishes right in the back of the wave crest and then converges again, especially with the lower frequency band (150Hz~ 600Hz). Azimuthal coherence estimated as a function of time-dependence is better in the lower frequencies (gained from 0.35 even to the 0.95 in the frequency of 150Hz and 800Hz at specified range, depth and azimuth) and also with increasing depth.(0.6~0.7 difference at deeper water column).

5 Reference

1. J. Lynch, S. Ramp, C. S. Chiu, T. Y. Tang, Y. J. Yang, and J. Simmen, "Research highlights from the Asian Seas International Acoustics Experiment in the South China Sea," *IEEE J. Oceanic Eng.*, vol. 29, pp. 1067-1074, Oct. 2004.
2. C. S. Chiu, S. Ramp, C. Miller, J. Lynch, T. Duda, and T. Y. Tang, "Acoustic intensity fluctuations induced by South China Sea internal tides and solitons," *IEEE J. Oceanic Eng.*, vol. 29, pp. 1249-1263, Oct. 2004.
3. T. Duda, J. Lynch, A. Newhall, L. Wu, and C. S. Chiu, "Fluctuation of 400-Hz sound intensity in the 2001 ASIAEX South China Sea Experiment," *IEEE J. Oceanic Eng.*, vol. 29, pp. 1264-1279, Oct. 2004.
4. S. Finette, M. H. Orr, A. Turgut, J. Apel, M. Badiey, C. S. Chiu, R. H. Headrick, J. N. Kemp, J. F. Lynch, A. E. Newhall, K. von der Heydt, B. Pasewark, S. N. Wolf, and D. Tielbuerger, "Acoustic field variability induced by time-evolving internal wave fields," *J. Acoust. Soc. Am.*, vol. 108, pp. 957-972, 2000.
5. D. Rubenstein, "Observations of cnoidal internal waves and their effect on acoustic propagation in shallow water," *IEEE J. Oceanic Eng.*, vol. 24, pp. 346-357, 1999.

6. R. Oba and S. Finette, "Acoustic propagation through anisotropic internal wave fields: TL, cross-range coherence, and horizontal refraction," *J. Acoust. Soc. Am.*, vol. 111, issue 2, pp. 769-784, 2002.
7. G. Botseas, D. Lee, and D. King, "FOR3D: A computer model for solving the LSS three-dimensional, wide angle wave equation," Naval Underwater Systems Center, TR 7943, 1987.
8. A. Tolstoy, "3-D Propagation Issues and Models," *J. Comput. Acoust.*, vol. 4, no. 3, pp. 243-271, 1996.
9. D. Lee and M. H. Schultz, "*Numerical Ocean Acoustic Propagation in Three Dimensions,*" Singapore: World Scientific, 1995, pp. 138-144.
10. S. Finette and R. Oba, "Horizontal array beamforming in an azimuthally anisotropic internal wave field," *J. Acoust. Soc. Am.*, vol.114, pp. 131-144, 2003.
11. K.B. Smith, C.W. Miller, A.F. D'Agostino *et al.*, "Three-dimensional propagation effects near the mid-Atlantic Bight shelf break (L)," *J. Acoust. Soc. Am.*, vol. 112, issue 2, pp. 373-376, 2002.
12. C. F. Chen and J. J. Lin, "Three Dimensional Effect on Acoustic Transmission in Taiwan's Northeastern Sea," *Proceedings of International Shallow-Water Acoustics*, Beijing, 1997.
13. C. F. Chen, J. J. Lin and T. Lee, "Acoustic transmission of Taiwan's northeast sea," *Acta Oceanographica Taiwanica*, no.34, pp.39-51, 1995.